

Adaptive Transmission Compensation via Human Visual System for Robust Single Image Dehazing

Zhigang Ling, Shutao Li, Yaonan Wang, Xiao Lu

College of Electrical and Information Engineering, Hunan University, Changsha, China

Abstract. Dark channel prior has been used widely in single image haze removal because of its simple implementation and satisfactory performance. However, it often suffers from halo artifacts or noise amplification, over-dark and over-saturation looking in some images containing heavy fog or large sky patches where dark channel prior is not established. To resolve these problems, this paper proposes a robust single dehazing algorithm via adaptive transmission compensation based on human visual system. The key contributions of this paper are made as follows: firstly, two boundary constraints on transmission map are deduced for the minimum intensity preservation and halo artifacts or noise suppression. Secondly, an improved HVS segmentation algorithm is employed to detect saturation areas in the input image. Finally, an adaptive transmission compensation method is present to remove fog in non-saturation areas and suppress the halo artifacts or noise in saturation areas. Experimental results indicate that this proposed method can robustly improve the visibility of the foggy image in the changing condition.

1 Introduction

In the past decades, restoration of images taken in hazy weather conditions has caught much attention due to the increasing outdoor applications, such as video surveillance, remote sensing, intelligent vehicles and object recognition and so on. In hazy weather conditions, the reflected light from these objects is attenuated in the air and further blended with the atmospheric light scattered by some aerosols (e.g., dust and water-droplets) before it reaches the camera, and for this reason, the colors of these objects fades and becomes much similar to the haze, which severely degrades the visibility of the captured scene.

In general, the haze is highly related to the scene depth and it is hard to estimate the scene depth from a single image, early haze removal methods usually rely on additional depth information or multiple images of the same scene. Schechner et al. [1] discover that the airlight scattered by atmospheric particles is partially polarized. Based on this observation, they develop a quick method to reduce hazes by using two images taken through a polarizer at different angles. Narasimhan et al. propose a physics-based scattering model [2] [3]. By this

model, the scene structure can be recovered from two or more weather images. Kopf et al. [4] propose to dehaze an image by using the scene depth information directly accessible in the georeferenced digital terrain or city models. However, additional depth information or multiple images are not available in many situations.

Recently, single image dehazing algorithms based on strong assumptions or constraints have been developed to overcome the limitation of the above-mentioned approaches. For example, Fattal[5] propose a refined image formation model to account for the surface shading and the scene transmission. Under the assumption that the two functions are locally statistically uncorrelated, a haze image can be decomposed into the albedo and the shading, and then the scene radiance is estimated via independent component analysis (ICA), from which the scene transmission can be inferred. It can remove haze locally but cannot restore densely hazy images. Tan[6] assumes that a haze-free image has a higher contrast ratio than the hazy image and maximizes the local contrast of a hazy image to remove haze from the input image, this method can generate quite satisfying results, especially in regions with dense haze. Meng et al. [7] model the boundary constraint and contextual regularization into an optimization problem to estimate the unknown scene transmission. However, the restored image often suffers from distorted colors and halos artifacts. He et al.[8] discover a interesting dark channel prior that at least one color channel of each pixel should have a small intensity value in a haze-free image, and estimate transmission for a hazy image based on this prior for haze removal. Due to the simply implementation and satisfactory performance of the dark channel prior, it has been widely used for different application[9][10][11][12]. For example, Zhang et al.[12] estimated an initial depth map for each frame of a video sequence using the dark channel prior, and then refined the depth map by exploiting spatial and temporal similarities for video dehazing. Tripathi et al.[13] use anisotropic diffusion for refining airlight map from dark channel prior to recover scene contrast. However, dark channel prior is often unavailable in the saturation regions, such as the sky or heavy haze patches. As a result, these methods based on dark channel priors suffer from the following problems: Firstly, the halo artifacts or image noise will be introduced in the saturation regions or distant sky patches where transmissions are very small, which will severely degraded image quality. Secondly, due to dark channel prior assumes that at least one color channel has a small pixel value in a haze-free image, the restored image often has a dark looking, which results in that some details cannot be discriminated.

To resolve two aforementioned problems, this paper proposes a robust single image dehazing method via transmission compensation based on human vision system (HVS), which firstly detects the saturated areas in the input images via human visual system. In order to suppress the halo artifacts and noise, this paper introduces the just-noticeable distortion (JND) of human visual system to decide the adaptive transmission compensation. Meanwhile, the brightness boundary constraint on transmission is employed to avoid producing the too dark

images. The experimental results show that the proposed algorithm efficiently and robustly both remove haze and suppress halo artifacts and noise.

2 Related works

Due to the absorption and scattering, the radiance from the objects through the atmosphere is attenuated and dispersed. In the hazy weather, dust, smoke, water droplets and other dry particles in the atmosphere greatly scatter, absorb the radiance from the objects in the scene and blend with the airlight and only a percentage of the reflected light reaches the observer causing poor visibility in such degraded scenes, which often yields low contrast and obscure the clarity of the sky[14]. According to the Koschmieder's law[15], the radiance that reaches the observer is composed of two main additive components: direct attenuation and veiling light[2]:

$$\mathbf{I}(\mathbf{x}) = \mathbf{L}(\mathbf{x})e^{-\beta d(\mathbf{x})} + \mathbf{A}(1 - e^{-\beta d(\mathbf{x})}) \quad (1)$$

where \mathbf{L} is the scene radiance, \mathbf{I} is the observed radiance, \mathbf{x} is the pixel position in the observed image, \mathbf{A} is the global airlight constant. The first component, direct attenuation $\mathbf{D} = \mathbf{L}(\mathbf{x})t(\mathbf{x})$, represents how the scene radiance is attenuated due to medium properties. The veiling light component is the main cause of the color shifting and can be expressed as:

$$\mathbf{V} = \mathbf{A}(1 - e^{-\beta d(\mathbf{x})}) = \mathbf{A}(1 - t(\mathbf{x})) \quad (2)$$

where $t(\mathbf{x}) = e^{-\beta d(\mathbf{x})} \leq 1$ is the transmission along the cone of vision and β is the homogeneous medium attenuation coefficient due to the scattering, while $d(\mathbf{x})$ represents the distance between the observer and the considered scene. The value of $t(\mathbf{x})$ depicts the amount of light that has been transmitted between the observer and the scene surface. The image hazing method aims to recover t , \mathbf{L} and \mathbf{A} for each pixel \mathbf{x} in the hazy image. Practically, while no additional information about depth and airlight are given, haze removal is an ill-posed problem.

He et al.[8] discover an interesting dark channel prior: in most of the non-sky patches of the haze-free image, at least one color channel has very low intensity at some pixels and defined the dark channel \mathbf{L}^{dark} of image \mathbf{L} as follows

$$\mathbf{L}^{dark} = \min_{y \in \Omega(\mathbf{x})} (\min_{c \in r, g, b} (\mathbf{L}_c(\mathbf{y}))) \quad (3)$$

where \mathbf{L}_c is a color channel of \mathbf{L} and $\Omega(\mathbf{x})$ is a local patch centered at \mathbf{x} . The dark channel operation is taken to the degraded model described in Eq.(1)

$$\min_{y \in \Omega(\mathbf{x})} (\min_{c \in r, g, b} (\frac{\mathbf{I}_c(\mathbf{y})}{\mathbf{A}_c})) = \min_{y \in \Omega(\mathbf{x})} (\min_{c \in r, g, b} (\frac{\mathbf{L}_c(\mathbf{y})}{\mathbf{A}_c})t(\mathbf{x}) + (1 - t(\mathbf{x}))) \quad (4)$$

Then, the estimated transmission map $t(\mathbf{x})$ can be described as

$$t(\mathbf{x}) = \frac{1 - \min_{y \in \Omega(\mathbf{x})} (\min_{\mathbf{c} \in r, g, b} (\frac{\mathbf{I}_c(\mathbf{y})}{\mathbf{A}_c}))}{1 - \min_{y \in \Omega(\mathbf{x})} (\min_{\mathbf{c} \in r, g, b} (\frac{\mathbf{L}_c(\mathbf{y})}{\mathbf{A}_c}))} \quad (5)$$

According to dark channel prior, for an outdoor haze-free image \mathbf{L} , its dark channel should tend to be zero and \mathbf{A}_c is positive constant, thus the estimated transmission can be simply determined by:

$$t_0(\mathbf{x}) = 1 - \min_{y \in \Omega(\mathbf{x})} (\min_{\mathbf{c} \in r, g, b} (\frac{\mathbf{I}_c(\mathbf{y})}{\mathbf{A}_c})) \quad (6)$$

Lastly, He et al. [8] used the soft matting to refine the estimated transmission and recover the clean image. However, this method cannot effectively suppress noise and halo artifacts. Based on the degraded model, the gradient magnitude of the hazy image and restored image has the following relationship [16].

$$\nabla \mathbf{I}_c(\mathbf{x}) = \nabla \mathbf{L}_c(\mathbf{x})t(\mathbf{x}) + \nabla \mathbf{A}_c(1 - t(\mathbf{x})) = \nabla \mathbf{L}_c(\mathbf{x})t(\mathbf{x}) \quad (7)$$

where ∇ denotes the gradient magnitude operator. Eq. (7) illustrates that the gradient magnitude in the restored image is related to the transmission. Due to the refraction or reflection of the water droplets in the atmosphere, the captured images often more or less suffer from the halo artifacts or noise, especially in the sky regions. In the foggy images, these halo artifacts or noises almost cannot be found because these gray differences cannot be perceived by human eyes. But, these imperceptible gray differences in the hazy image will be greatly boosted after the fog removal because the transmission is close to zero, and then halo artifacts are introduced into the restored images after the haze removal. As shown in Fig.1(b), some halo artifacts are introduced in the sky regions. Similarly, image noise is also extremely magnified, all this severely degrade the restored images. Moreover, dark channel prior assumes that at least one color channel of the haze-free image \mathbf{L} should tend to be zero, which will darken the restored images. To deal with the aforementioned problems, in this paper, we propose a robust single image dehazing method via adaptive transmission compensation. Fig.1 illustrates an example of our dehazing result.

3 The proposed method

3.1 Boundary constraint on transmission

Geometrically, according to Eq.(1), a pixel $\mathbf{I}(\mathbf{x})$ contaminated by haze will be "pushed" towards the global atmospheric light \mathbf{A} [7]. As a result, the clean pixel $\mathbf{L}(\mathbf{x})$ can be recovered by a linear extrapolation from \mathbf{A} to $\mathbf{I}_c(\mathbf{x})$. Consider that the scene radiance of a given image is always bounded, that is,

$$\mathbf{L}(\mathbf{x}) \geq \mathbf{L}^0(\mathbf{x}) \quad (8)$$

where $\mathbf{L}^0(\mathbf{x})$ is a lower bound vector that is relevant to the given image. Consequently, for any pixel \mathbf{x} , a natural requirement is that the extrapolation of $\mathbf{L}(\mathbf{x})$

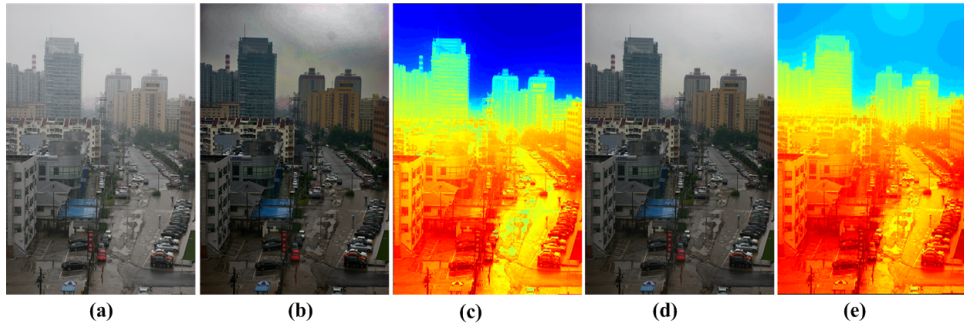


Fig. 1. Comparison with the method of He's work, (a) input image *Street*, (b) the result of He's work, (c) the transmission estimated by He's work, (d) the result of our method, (e) the transmission estimated by our method.

must be larger than the lowest intensity bounded by \mathbf{L}^0 . In turn, given the global atmospheric light \mathbf{A} and the lower bound vector $\mathbf{L}^0(\mathbf{x})$, a boundary constraint on $t(\mathbf{x})$ by the lowest intensity can be determined as

$$t(\mathbf{x}) \geq t_b(\mathbf{x}) = \frac{1 - \min_{y \in \Omega(\mathbf{x})} (\min_{\mathbf{c} \in r, g, b} (\frac{\mathbf{I}_c(\mathbf{y})}{\mathbf{A}_c}))}{1 - \min_{y \in \Omega(\mathbf{x})} (\min_{\mathbf{c} \in r, g, b} (\frac{\mathbf{L}_c^0(\mathbf{y})}{\mathbf{A}_c}))} \geq t_0(\mathbf{x}) \quad (9)$$

where $t_b(\mathbf{x})$ is the lower bound of $t(\mathbf{x})$ bounded by \mathbf{L}^0 .

According to Formula (8), the halo artifacts in the sky patches originate from the enlarged gray difference between neighboring pixels in the hazy image. Therefore, another constraint for the halo artifacts and image noise suppression should be imposed on transmission so that no local luminance variation is also perceived in the restored image if no local luminance variation is perceived in the hazy image. This paper introduces the just-noticeable difference or distortion (JND) model of the human visual system (HVS) to adaptively decide the boundary constraint on transmission.

JND model is a quantitative measure for distinguishing the luminance change perceived by the HVS[17][18]. That is to say, JND gives the maximum difference of the luminance values that cannot be perceived by human eyes and the perceptual function for evaluating the visibility threshold of the JND model can be described by the following equation:

$$JND(k) = \begin{cases} T_0 [1 - (k/127)^{0.5}] + 3 & k < 127 \\ \gamma(k - 127) + 3 & otherwise \end{cases} \quad (10)$$

where k is the background luminance within $[0, 255]$ and the parameters T_0 and γ depend on the viewing distance between the objects and the observer. T_0 denotes the visibility threshold when the background gray level is 0, and γ denotes the slope of the line that models the JND visibility threshold function at higher background luminance. In this work, T_0 and γ are set to be 17 and

3/128 based on the subjective experiments conducted by Chou and Li[17]. It is easy to verify that the HVS perceives the luminance variation best in the situation where the background luminance is 127. In other words, if the HVS cannot perceive the luminance variation where the background luminance is 127, it cannot perceive the luminance variation in the other situations either. Moreover, the background luminance is approximately linear to the luminance variation since the pixel luminance is linear to the background luminance.

Due to the scene radiance of a given image is always bounded, luminance variation is also bounded. Therefore, based on the HVS, the luminance variation and the corresponding background intensity of the recovered image often meet the following condition:

$$\frac{\Delta \mathbf{L}(\mathbf{x})}{\mathbf{L}(\mathbf{x})} = \frac{\Delta \mathbf{I}(\mathbf{x})/t(\mathbf{x})}{(\mathbf{I}(\mathbf{x}) - \mathbf{A})/t(\mathbf{x}) + \mathbf{A}_c} = \frac{\Delta \mathbf{I}(\mathbf{x})}{\mathbf{I}(\mathbf{x}) - \mathbf{A} + \mathbf{A}t(\mathbf{x})} \leq \frac{V}{127} \quad (11)$$

where V is the sensing threshold and $\Delta \mathbf{L}(\mathbf{x})$ is luminance variation computed by the difference between the luminance $\mathbf{L}(\mathbf{x})$ and the corresponding low-pass filtered value, the intensity value 127 is used as the ideal background luminance to detect the maximum amount of details. In turn, Formula (13) imposes this constraint on $t(\mathbf{x})$ as follows:

$$t(\mathbf{x}) \geq t_0(\mathbf{x}) + \frac{127\Delta \mathbf{I}(\mathbf{x})}{V\mathbf{A}} \geq 1 - \frac{\mathbf{I}(\mathbf{x})}{\mathbf{A}} + \frac{127\Delta \mathbf{I}(\mathbf{x})}{V\mathbf{A}} \quad (12)$$

Thus, transmission compensation to the estimated transmission $t_0(\mathbf{x})$ is given by:

$$\Delta t(\mathbf{x}) = \frac{127}{V} \max_{y \in \Omega(\mathbf{x})} \max_{c=r,g,b} \left(\frac{\Delta \mathbf{I}_c(\mathbf{y})}{\mathbf{A}_c} \right) = \frac{127}{V} \mathbf{G}^{bright}(\mathbf{x}) \quad (13)$$

where $\mathbf{G}^{bright}(\mathbf{x})$ is the bright channel of the normalized variation and defined as follows:

$$\mathbf{G}^{bright}(\mathbf{x}) = \max_{y \in \Omega(\mathbf{x})} \max_{c=r,g,b} \left(\frac{\Delta \mathbf{I}_c(\mathbf{y})}{\mathbf{A}_c} \right) \quad (14)$$

Obviously, supposing the threshold V is given, in order to retain halo artifacts, the larger the luminance variation value is, the more compensation is needed. But in the non-saturation regions, image dehazing aims to remove haze as cleanly as possible so that the recovered image has high contrast and the details can be clearly discriminated, and no transmission compensation is needed. In other word, the threshold V should keep large value so that $\Delta t(\mathbf{x})$ should be approximates to zero and no transmission compensation is needed. On the contrary, as for the distant sky region, the threshold V cannot be larger than the visibility threshold defined by JND model. Due to different transmission compensation strategies are taken in different regions to both suppress halo artifacts and remove haze. Therefore, it is a key problem to segment saturation and non-saturation regions. In the Section 3.2, this paper will introduce the saturation regions detection method based on the HVS.

3.2 Saturation areas detection based on HVS

In fact, the fog or haze has similar qualities with human visual areas including Devries-Rose, Weber, saturation and low contrast areas[21]. Specifically, the heavy hazy image has high brightness, concentrated gray distribution in the saturation regions and these pixels with thin haze tend to be concentrated in the Devries-Rose regions and these pixels with moderate haze are concentrated in the Weber regions. In a word, three areas of the human visual system, Devries-Rose, Weber and saturation area are corresponding to different thickness of haze: thin, moderate and heavy haze, respectively. Based on this property, we utilized the HVS to divide the hazy image into the saturation and non-saturation regions.

According to Ref.[19], HVS image enhancement performs this segmentation using the background intensity and the rate of change information. The background intensity is calculated as a weighted local mean, and the rate of change is calculated as a gradient measurement. The background intensity at each pixel \mathbf{x} is derived by using the following formula,

$$\mathbf{B}(\mathbf{x}) = m \otimes \left[m \otimes \left(\frac{m}{2} \otimes \sum_{y \in \mathbf{Q}^D(\mathbf{x})} \mathbf{I}(\mathbf{y}) \right) \oplus \mathbf{I}(\mathbf{x}) \right] \quad (15)$$

where $\mathbf{B}(\mathbf{x})$ is the background intensity of luminance component at pixel \mathbf{x} , $\mathbf{I}(\mathbf{x})$ is the luminance component of input image, $\mathbf{Q}(\mathbf{x})$ is the set of the pixels which are directly up, down, left, and right from the pixel, $\mathbf{Q}^D(\mathbf{x})$ is all of the pixels diagonally one pixel away, m and n some constant. \oplus and \otimes is the PLIP model operator and can be summarized as follows:

$$a \oplus b = a + b - \frac{ab}{M} \quad (16)$$

$$c \otimes a = M - M * \left(1 - \frac{a}{M}\right)^c \quad (17)$$

where M is the maximum value of the range. Finally, these threshold parameters concerning human eye itself for different regions segmentation are given as follows:

$$B_1 = \alpha_1 B_T \quad B_2 = \alpha_2 B_T \quad B_3 = \alpha_3 B_T \quad (18)$$

where α_1 , α_2 is the lower contrast level, Devries-Rose and Weber level, respectively. α_3 is the saturation level and. B_T is the maximum difference threshold.

In the saturation regions, the intensity $\mathbf{I}(\mathbf{x})$ for each pixel in the hazy image is close to airlight and also is larger than the threshold B_3 as defined in Ref.[19], and the transmission tends to be close to zeros. Moreover, these halo artifacts and image noise cannot be perceived in the original images, which means the corresponding luminance variation is smaller than the visibility threshold defined in Eq.(12). Therefore, unlike to Ref.[19], this paper defines the condition of saturation areas or sky patch as follows:

$$\mathbf{x} \in \begin{cases} \mathbf{S} & \text{if } : t_0(\mathbf{x}) \leq T_h \quad \mathbf{I}(\mathbf{x}) \geq B_3 \quad \Delta\mathbf{I}(\mathbf{x}) < J_{nd} \\ \mathbf{Other} & \text{otherwise} \end{cases} \quad (19)$$

where \mathbf{S} denotes the saturation region, T_h and J_{nd} is the transmission, visibility threshold, respectively. Based on Eq.(22), the hazy image is firstly divided into two regions of human visual response. Some segmentation results are shown in Fig. 2, which indicates the improved method can efficiently and robustly segment saturation regions.

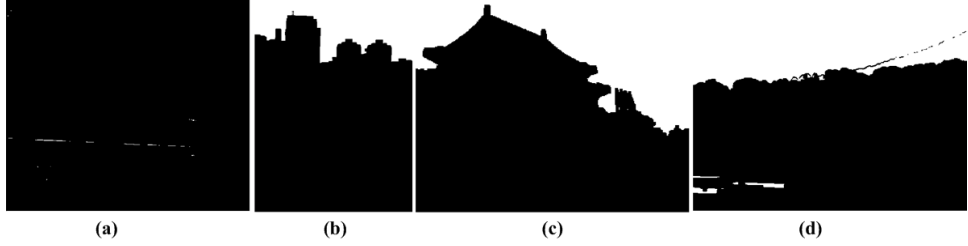


Fig. 2. Image segmentation results by our method for haze images *Canon*, *New York*, *Sam* and *Traffic* (The original images are shown in Fig.3-Fig.5).

3.3 Adaptive transmission compensation

According to Eq.(15), the threshold V should keep large value for the non-saturation regions and no transmission compensation is needed so that the haze can be removed as cleanly as possible. On the contrary, as for these pixels in the saturation regions, in order to retain halo artifacts, the threshold V cannot be larger than the visibility threshold defined by JND model. At the same time, in order to maintain the continuity of the transmission compensation, we set the transmission compensation intensity variation for a pixel \mathbf{x} as

$$\Delta t_1(\mathbf{x}) = \frac{127}{V} \max_{y \in \Omega(\mathbf{x})} \max_{c=r,g,b} \left(\frac{\Delta\mathbf{I}_c(\mathbf{y})}{\mathbf{A}_v} \right) = \frac{127}{V_h + (V_l - V_h) \frac{\mathbf{I}^{dark}(\mathbf{x})}{\max(\mathbf{I}^{dark})}} \mathbf{G}_0^{bright}(\mathbf{x}) \quad (20)$$

where V_l, V_h is the lower and higher bound of the sensing threshold, respectively. $\mathbf{G}_0^{bright}(\mathbf{x})$ is the modified bright channel of the normalized variation, and described as

$$\mathbf{G}_0^{bright}(\mathbf{x}) = \begin{cases} \frac{Y_{max}}{\mathbf{A}^{dark}} & \mathbf{G}^{bright}(\mathbf{x}) > \frac{J_{max}}{\mathbf{A}^{dark}} \cap \mathbf{x} \in \mathbf{S} \\ \frac{Y_{min}}{\mathbf{A}^{dark}} & \left(\mathbf{G}^{bright}(\mathbf{x}) < \frac{J_{min}}{\mathbf{A}^{dark}} \cap \mathbf{x} \in \mathbf{S} \right) \cup (\mathbf{x} \notin \mathbf{S}) \end{cases} \quad (21)$$

where J_{max} , J_{min} is the maximum and minimums perceptual threshold, respectively, because the pixels in the hazy image have different intensity variation $\mathbf{G}^{bright}(\mathbf{x})$ and the over-large or over-small intensity variations are not beneficial to the haze removal and the halo artifacts or noise suppression. Hence, J_{max} and J_{min} are used to confine the intensity variation of the pixels so that little transmission compensation is exerted to the pixels in the non-saturation regions and much transmission compensation is applied to the pixels in the saturation regions for halo artifacts or noise suppression

Moreover, the brighter the dark channel is, the more compensation is needed, vice versa. Thus, we define the transmission compensation based on dark image for each pixel as follows:

$$\Delta t_2(\mathbf{x}) = w(\mathbf{x})\Delta T = \exp\left(\frac{I^{dark}(\mathbf{x}) - I_{max}}{\sigma_2}\right)\Delta T \quad (22)$$

where I_{max} is the upper bound of the gray value and is set to 255 in this paper and ΔT is the maximum transmission compensation value and given by $\Delta T = 127 * J_{max}/(V_l * \mathbf{A}^{dark})$, σ_2 is suggested be $0.2I_{max}$. Thus, by integrating the above-mentioned two transmission compensations, the final transmission compensation can be made by the following function:

$$\Delta t(\mathbf{x}) = \max(\Delta t_1(\mathbf{x}), \Delta t_2(\mathbf{x})) \quad (23)$$

At the same time, in order to avoid the transmission value is larger than one, the compensated transmission is redefined as

$$t_1(\mathbf{x}) = t_0(\mathbf{x}) + \min(\Delta t(\mathbf{x}), 1 - t_0(\mathbf{x})) \quad (24)$$

Furthermore, in order to avoid to recover the too dark images, transmission also should meet this condition given by Eq.(10). Therefore, the final estimated transmission is given by

$$t(\mathbf{x}) = \max(t_b(\mathbf{x}), t_1(\mathbf{x})) \quad (25)$$

Lastly, this paper adopts the guided filter[20] to refine the final estimated transmission map and restore the clear images.

4 Experimental results

In order to comprehensively demonstrate the effectiveness and robustness of this proposed algorithm, firstly, this paper qualitatively evaluates the performance of this proposed algorithm on a group of typical images. Secondly, this study quantitatively compares this proposed algorithm with several state-of-the-art methods. All algorithms were performed in Matlab by using a 32bit desktop with an Intel Pentium dual-core 3.2 GHz CPU and 2G RAM. In saturation regions detection algorithm, the parameters m , n , M , α_3 and β are set as 0.9, 1.4, 255, 0.9 and 0.2, respectively. The visibility threshold J_{nd} is set to 3 and

the boundary constraint map is computed from by setting the radiance bounds $\mathbf{L}^0 = (30, 30, 30)$. The sensing threshold V_l, V_h are set as 3, 80 and the perceptual threshold J_{max} and J_{min} are set as 3, 1, respectively. The airlight \mathbf{A} is estimated via He’s work.

4.1 Qualitative evaluation

Fig. 3 gives some examples of our dehazing results and the recovered scene transmission maps on the natural hazy images with different size of saturation regions. Obviously, the results show that proposed algorithm restores hazy images very well with acceptable visual quality: haze is almost completely removed in image *Canon* which has no sky patches, and no distinct halo artifacts or noises are introduced into the sky patches for the image *NewYork*, *Sam* and *Traffic* when haze is removed, because the proposed method adaptively compensate the transmission in the sky patches, which can effectively remove haze and suppress halo artifacts and noises.

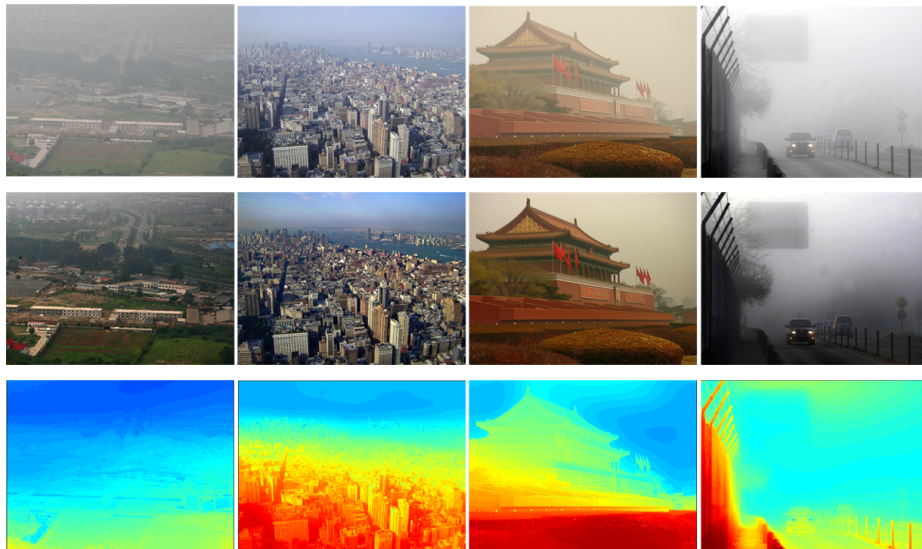


Fig. 3. Image dehazing results by our method. Top: input haze images *Canon*, *NewYork*, *Sam* and *Traffic*. Middle: the dehazing results. Bottom: the recovered transmission maps.

We also compare our method with several state-of-the-art methods. Fig. 4 and 5 illustrate the comparisons of our method with He’s[8], Tarel’s[21], Fattal’s[5], Tripathi’s[13], Meng’s[7] methods. As for the hazy image shown in Fig.4(a), Tarel’s method can augment the image details and enhance the image visibility. However, some white artifacts usually appear around the sharp edges (e.g.,

trees). Fattal’s method darkens some regions of image(e.g., trees regions). Meng’s methods produce the excessive saturated color images. The proposed method produces the similar result to He’s method because it makes a little compensation to the transmission. Fig.5(a) depicts a forest region against a background of bright sky. Tarel’s and Tripathi’s method not only introduce white artifacts around the sharp edges but also generate some halo artifacts in the sky patches. Fattal’s method over-enhances the sky. He’s and Meng’s produce the saturated color and low-lighting images, meanwhile, they introduce significant halo artifacts in the sky. In comparison, our method not only removes the haze in the hazy image, but also suppresses the halo artifacts in the sky patches, which improves the visual quality of image while restoring the faithful colors and preserves the structure information and appropriate brightness of the original image.



Fig. 4. Comparison with image dehazing results of state-of-the-art algorithms on image *House*, (a)input image, (b) He’s result, (c)Tarel’s result, (d) Fattal’s result, (e) Meng’s result and (f) Our result .

4.2 Quantitative evaluation

Because it is difficult to acquire the corresponding ground truth data for the input foggy images, this paper uses two quantitative evaluation metrics to quantitatively assess this proposed algorithm and compare it with these state-of-the-art algorithms[11], these evaluation metrics are named as the new visible edges ratio (e) and structure similarity (S_s). The metric e proposed by Hautiere et al.[22] evaluates the ability of the method to restore edges which are not visible in original image but are visible in restored image, the higher metric e indicates the better performance of the image dehazing algorithm because clean images have more contrast than images plagued by haze. The structure similarity (S_s) present by Wang et al.[23] evaluates the structure perseveration of the dehazing method because the dehazed images should generally maintain the similar structure information to the original images, and the low structure similarity often means the over-enhancement and the introduction of halo artifacts or noise,vice versa.

A comparison between our proposed method and other methods on the above-mentioned hazy images is made and shown in Table 1. Tripathi’s method

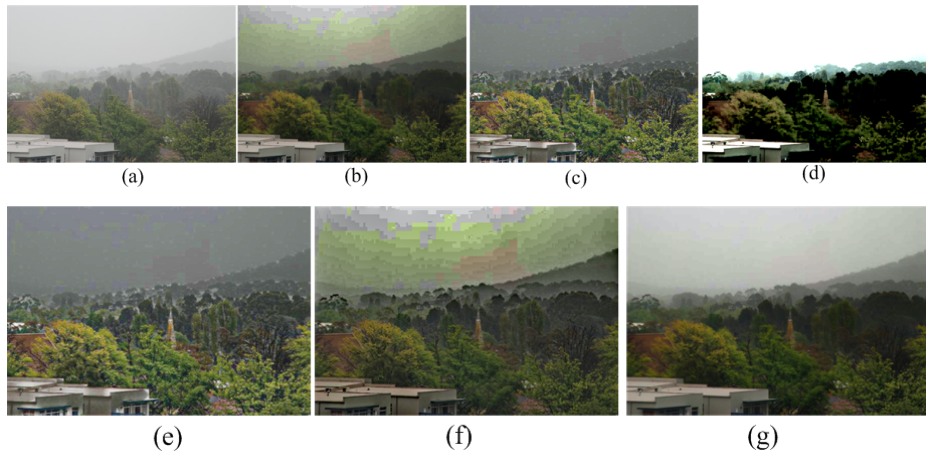


Fig. 5. Comparison with image dehazing results of state-of-the-art algorithms on image *Canberra*. (a)input image, (b) He's result, (c)Tarel's result, (d)Fattal's result, (e) Tripathi's result, (f) Meng's result and (g) Our result

nearly gives the highest metric e because it has the high brightness value. Tarel's and Fattal's method even degrade the hazy images, e.g., image *Traffic*. Compared with He's and Meng's method, the proposed algorithm greatly improves the image contrast although it has the lowest metric e which is mainly caused by little distinct halo artifacts introduced in the sky patches. Moreover, the proposed algorithm has the highest structure similarity, which shows it has better performance of halo artifacts or noise suppression.

Table 1. Quantitative Comparisons in e and Ss

Image	Canberra		Canon		Sam		House		Traffic		Street		New York	
	e	Ss	e	Ss	e	Ss	e	Ss	e	Ss	e	Ss	e	Ss
He	1.01	0.83	9.83	0.80	0.96	0.77	0.52	0.94	2.27	0.74	0.83	0.86	0.72	0.88
Fattal	0.60	0.59	13.2	0.53	1.16	0.50	1.10	0.66	-0.01	0.77	0.75	0.00	0.92	0.14
Tarel	1.39	0.78	4.27	0.73	1.23	0.74	0.94	0.89	-1.00	0.00	1.04	0.79	0.66	0.82
Tripathi	3.76	0.44	12.5	0.46	1.28	0.56	1.12	0.85	6.28	0.27	2.12	0.57	1.43	0.67
Meng	1.29	0.78	8.80	0.80	0.78	0.76	0.66	0.96	3.32	0.64	1.15	0.84	0.81	0.87
Our	0.76	0.87	7.42	0.81	0.85	0.81	0.40	0.95	1.45	0.79	0.63	0.89	0.60	0.89

5 Conclusions

This paper develops a robust single-image dehazing algorithm using adaptive transmission compensation via human visual system. This paper firstly employs an improve segmentation method based on HVS to decompose the hazy image into saturation and non-saturation regions. Then, an adaptive transmission compensation method via just-noticeable distortion (JND) of human visual system is present to suppress the halo artifacts and noise. Meanwhile, the brightness boundary constraint on transmission is employed to avoid producing too dark restored images. Experimental results on a variety of haze images demonstrate the proposed method can robustly produce the high quality images in various realistic scenes.

Acknowledgement. This work was supported by the National High Technology Research and Development Program of China (863 Program, Grant No. 2012AA112312), National Natural Science Foundation of China (Grant No. 61471166, 61175075, 61374023), and the Science and Technique Project of Ministry of Transport of the People’s Republic of China (Grant No. 201231849A70)..

References

1. Schechner, Y.Y., Narasimhan, S.G., Nayar, S.K.: Polarization-based vision through haze. *Applied Optics* **42** (2003) 511–525
2. Narasimhan, S.G., Nayar, S.K.: Contrast restoration of weather degraded images. *IEEE Transactions on Pattern Analysis and Machine Intelligence* **25** (2003) 713 – 724
3. Narasimhan, S.G., Nayar, S.K.: Vision and the atmosphere. *International Journal on Computer Vision* **48** (2002) 233–254
4. Kopf, J., Neubert, B., Chen, B., Cohen, M.F., Cohen-Or, D., Deussen, O., Uyttendaele, M., Lischinski, D.: Deep photo: Model-based photograph enhancement and viewing. *ACM Transactions on Graphics (Proceedings of SIGGRAPH Asia 2008)* **27** (2008) 116:1–116:10
5. Fattal, R.: Single image dehazing. *ACM Transactions on Graphics* **27** (2008) 721–729
6. Tan, R.T.: Visibility in bad weather from a single image. In: *Proceedings of IEEE Conference on Computer Vision and Pattern Recognition (CVPR)*, New York, USA (2008) 2347–2354
7. Meng, G., Wang, Y., Duan, J., Xiang, S., Pan, C.: Efficient image dehazing with boundary constraint and contextual regularization. In: *Proceedings of IEEE International Conference on Computer Vision (ICCV)*, Sydney, NSW (2013) 617–624
8. He, K., Sun, J., Tang, X.: Single image haze removal using dark channel prior. In: *Proceedings of IEEE Conference on Computer Vision and Pattern Recognition*. Volume 1. (2009) 1956–1963
9. Inhye, Y., Seonyung, K., Donggyun, K., Hayes, M.H., Joonki, P.: Adaptive defogging with color correction in the hsv color space for consumer surveillance system. *IEEE Transactions on Consumer Electronics* **58** (2012) 111–116
10. Xie, B., Guo, F., Cai, Z.: Universal strategy for surveillance video defogging. *Optical Engineering* **51** (2012) 1017031–1017037

11. Sun, W., Guo, B.L., Li, D.J., Jia, W.: Fast single-image dehazing method for visible-light systems. *Optical Engineering* (2013)
12. Zhang, J., Li, L., Zhang, Y., Yang, G., Cao, X., Sun, J.: Video dehazing with spatial and temporal coherence. *The Visual Computer* **27** (2011) 749–757
13. Tripathi, A.K., Mukhopadhyay, S.: Single image fog removal using anisotropic diffusion. *IET Image Processing* **6** (2012) 966–975
14. J., M.E.: *Optics of Atmosphere: Scattering by Molecules and Particles*. New York: John Wiley and Sons (1976)
15. Koschmieder, H.: Theorie der horizontaler sichtweite beitraege. *Physicae Freiburger Atmosphere* (1925) 33–55
16. Li, W.J., Gu, B., Huang, J.T., Wang, S.Y., Wang, M.H.: Single image visibility enhancement in gradient domain. *IET Image Processing* **6** (2012) 589–595
17. Chou, C.H., Li, Y.C.: A perceptually tuned subband image coder based on the measure of just-noticeable-distortion profile. *IEEE Transactions on Circuits and Systems for Video Technology* **5** (1995) 467–476
18. Lee, C.H., Lin, P.Y., Chen, L.H., Wang, W.K.: Image enhancement approach using the just-noticeable-difference model of the human visual system. *Journal of Electronic Imaging* **21** (2012) 033007
19. Panetta, K.A., Wharton, E.J., Agaian, S.S.: Human visual system-based image enhancement and logarithmic contrast measure. *IEEE Transactions on Systems, Man, and Cybernetics, Part B: Cybernetics* **38** (2008) 174–188
20. He, K., Sun, J., Tang, X.: Guided image filtering. *The 11th European Conference on Computer Vision (ECCV)* (2010)
21. J, P.T., Hautiere., N.: Fast visibility restoration from a single color or gray level image. In: *Proceedings of IEEE International Conference on Computer Vision, New York, USA* (2009) 2201–2208
22. Hautire, N., Tarel, J.p., Aubert, D., Dumont, r.: Blind contrast enhancement assessment by gradient ratioing at visible edges. *Image Analysis and Stereology* **12** (2008) 87–95
23. Wang, Z., Bovik, A.C., Sheikh, H.R., Simoncelli, E.P.: Image quality assessment: from error visibility to structural similarity. *IEEE Transactions on Image Processing* **13** (2004) 600–12